Morphology and Mechanical Properties of Soy Protein Scaffolds Made by Directional Freezing

Juan Guan,[1,2] David Porter,[2] Kun Tian,[1] Zhengzhong Shao,[1] Xin Chen[1]

[1]*The Key Laboratory of Molecular Engineering of Polymers of Ministry of Education, Department of Macromolecular Science, Laboratory of Advanced Materials, Fudan University, Shanghai 200433, China*
[2]*Department of Zoology, University of Oxford, Oxford OX1 3PS, United Kingdom*

Received 29 January 2010; accepted 2 April 2010
DOI 10.1002/app.32579
Published online 3 June 2010 in Wiley InterScience (www.interscience.wiley.com).

ABSTRACT: Directional freezing and freeze-drying techniques were used to make robust soy protein scaffolds. The development of the morphology and mechanical properties of the scaffolds with fabrication conditions such as solution concentration and freeze temperature was studied in detail. Directional freezing produced anisotropic morphological features in the soy protein scaffolds, which produced differences between the mechanical properties in the freeze direction and the direction perpendicular to it. The evolution of the scaffold morphology started from the fibrillar columns, which widened to become layers and which then grew regularly spaced ridges normal to the layers, which eventually fused to form a highly anisotropic foam structure. Suitable soy protein solutions for making the scaffolds were prepared with guanidine hydrochloride and dithiothreitol, and the viscosity–concentration relations showed that the soy protein behaved consistently as a good polymer solution over the concentration range used for the scaffolds. © 2010 Wiley Periodicals, Inc. J Appl Polym Sci 118: 1658–1665, 2010

Key words: biopolymers; mechanical properties; morphology; structure–property relations

INTRODUCTION

As part of the growing concern for energy and raw material resources and waste disposal, there has been great interest in the development and application of renewable biopolymers that are also biodegradable. Soy protein has been used widely in the food industry because of its great nutritional value. However, demand is now developing to examine new industrial uses of soy protein because of its sustainability, abundance, low cost, and functionality.[1] Generally, soy-protein-based materials can be divided into three groups: plastics,[2–4] gels,[5,6] and additives or coatings.[7,8] For many years, researchers have looked to improve the properties and functionality of soy-protein-based materials. Soy protein plastics, for example, are modified chemically and blended with synthetic or other natural polymers to overcome their fundamental limitations, including water sensitivity and poor processability and strength.[2,9,10] However, these disadvantages are such that far more work is needed before soy protein polymers are likely to be used in commercial applications requiring good structural properties.

To this point, there have been few reports on soy protein porous materials. In this article, we demonstrate novel methods for making porous soy protein scaffolds. Most importantly, soy proteins have shown their potential in the biomedical field and for organic–inorganic composites.[11–13] Freezing and freeze-drying is a simple technique for obtaining porous or layered materials with fine microstructures from two-phase systems (aqueous or organic solutions, suspensions, and slurries). When the freezing of a solvent or liquid phase is done in a definite direction, we call the process *directional freezing*. Directional freezing has been used to make a range of advanced materials.[14] Deville and coworkers[15,16] fabricated nacre-like alumina–Al–Si composites and hydroxyapatite scaffolds with strengths up to four times higher than currently used implantation materials using the freeze-casting method. Other researchers have succeeded in making porous chitosan,[17] poly(vinyl alcohol), and poly (ε-caprolactone) aligned scaffolds.[18] However, natural polymers, especially globular proteins, have rarely been made into materials through the directional-freezing technique.

Correspondence to: X. Chen (chenx@fudan.edu.cn).
Contract grant sponsor: National Natural Science Foundation of China; contract grant number: 20674011.
Contract grant sponsor: Program for New Century Excellent Talents in University of Ministry of Education of China; contract grant number: NCET-06-0354.
Contract grant sponsor: Program for Changjiang Scholar and Innovative Research Team in University of Ministry of Education of China; contract grant number: IRT-06-12.

In this study, a low-cost biodegradable polymer, soy protein isolate (SPI; a commercial purification product of soy protein), was processed by directional freezing to form scaffolds with aligned morphologies. The first step was to find a way to dissolve the complex mixture of globular proteins in the SPI into a solution form that could be used to prepare mechanically robust scaffolds. Two key processing factors were then studied, the freezing rate and the initial concentration, for their effect on the morphology and mechanical properties of the porous scaffolds. Furthermore, an analysis of the structure–property relations in the scaffolds revealed some interesting and unexpected aspects of the novel scaffold materials, which are considered here as anisotropic open-cell foams.

EXPERIMENTAL

Preparation and characterization of the SPI solution

SPI (purchased from Shenyuan Co., Shanghai, China) was dissolved in a 6 mol/L guanidine hydrochloride (GuHCl; purchased from Sinopharm Chemical Reagent Co., Shanghai, China) aqueous solution with 25 mmol/L dithiothreitol (DTT; purchased from Shanghai Boyun Biotechnology Co., Shanghai, China) to break the disulfide bonds. The solution was dialyzed against sodium hydroxide aqueous solutions and then against deionized water to neutralize it. The final SPI solution, with a concentration of about 2 wt % at a pH of about 8, was obtained. Concentrated solutions with different concentrations were prepared with reverse osmosis against a 10% poly(ethylene glycol) solution. The solutions were prepared at room temperature and stored at 4°C for further use. The reason we stored the soy protein solutions at 4°C was that soy proteins are vulnerable to bacteria if stored at room temperature. This solution method, developed as part of this study, was described elsewhere.[19] The viscosity profiles of the SPI solutions with different concentrations were measured on a Bohlin Gemini HR Nano 200 (Malvern Instruments, United Kingdom).

Preparation and characterization of the SPI scaffolds

SPI solutions (0.785 mL) with different concentrations were placed in cylinders with a diameter of 10 mm and a depth of 15 mm with polytetrafluoroethylene walls, which prevented perpendicular thermal transfer, and a copper bottom to provide good heat exchange with the freezing bath. The cylinders were then placed in the freezing baths only with their copper bottoms immersed. The temperatures of the freezing baths were about −196°C [liquid nitrogen (LN_2)], −96°C [freezing ethanol (EtOH)], and −50°C [freezing ethyl acetate (EtAc)]. The SPI solutions were directionally frozen from the bottom up.

After the solutions were completely frozen, the cylinders with SPI–ice composites were moved immediately to the freeze drier at a temperature of −50°C and a pressure of 10 Pa to sublimate the ice. The resultant samples were cylindrical SPI scaffolds with diameters of about 10 mm and lengths of about 10 mm.

The mechanical properties of the SPI scaffolds with good cylindrical form were tested on an Instron 1122 machine (Norwood, MA) in compression mode at a rate of 1.0 mm/s. The dimensions of all of the samples were measured with a vernier caliper. Scanning electron microscopy tests were conducted on a Philips XL30 (Almelo, The Netherlands) instrument with an acceleration voltage of 20 kV. The morphological features of samples cut in both the freeze direction and perpendicular direction were photographed.

RESULTS AND DISCUSSION

SPI solution

Commercially available SPIs are difficult to dissolve in water.[20] Screening trials in this study showed that the quality of the soy protein solutions used to prepare the scaffolds was important and that poor solutions of the normally globular protein gave very poor mechanical properties and were not robust enough for characterization. GuHCl and DTT are commonly used to denature proteins without degrading the peptide chain structure.[21,22] The GuHCl removed the strong interchain hydrogen bonding, and the DTT broke the interchain disulfide covalent bonds in the 11S fraction; this allowed the normally globular soy protein chains to dissolve at neutral pH levels, and this approach was presented in detail elsewhere.[19] The resulting solution was composed mainly of the dissolved subunits of the 7S and 11S fractions with molecular weights ranging from 20 to 71 kD[23,24] and an estimated weight-average molecular weight of about 41 kD. This should have been sufficient for robust polymer films because the weight-average molecular weight was greater than five times the estimated entanglement molecular weight of about 7 kD.[25]

From the viscosity–shear rate profiles of the soy protein solutions over the range of concentrations used in this study (3–14 wt %), we found that the viscosity–concentration relation at lower shear rates of around 0.1 s^{-1} had an approximately power 5 dependence on the concentration (Fig. 1). This implied that our soy bean solution was a well-dissolved molecular solution[26] rather than a suspension of

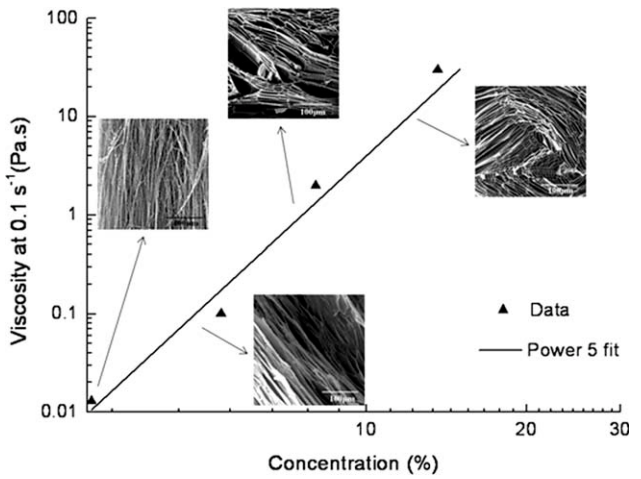

Figure 1 Viscosity–shear rate profile for different solution concentrations used in the scaffold preparation with a viscosity–concentration plot at 0.1 s^{-1} showing a power 5 relation, which indicates good solubility.[26] The inserted pictures show typical scaffold morphologies derived from the solutions defined by the concentration or viscosity as the arrows indicate.

globular protein that had strong intrachain interactions, such as hydrogen bonding and hydrophobic interactions.[27] These results show that the soy protein solution behaved consistently over the range of concentrations used in this study to produce scaffolds. At concentrations greater than 14 wt %, the solutions became gels and did not give the desired uniaxial scaffold morphologies. Figure 1 also shows how the typical morphologies of SPI scaffolds developed as the concentration or viscosity of the solution increased.

Strategy for making the SPI scaffolds

In the preparation for SPI scaffolds, the SPI solution was first frozen by directional freezing in different freezing baths. The ice was then removed from the solid system by freeze drying. The phase diagram is shown schematically in Figure 2.

In the first step, water molecules grew into ice, and the ice template played a key role in the formation of the morphology of the SPI scaffolds. Under normal pressure and at 120–265 K, the ice grew in the hexagonal crystalline form and had a morphology of pillars or lamellae. With the freezing applied in a definite direction, the ice crystals grew preferentially along this direction. In Deville and coworkers' experiment,[15,16] the temperature gradient of freezing was fixed to some extent by gradual immersion of the container into the freezing bath to maintain the dimensions of the freezing zone. In our study, the temperature gradient (the driving force of freezing) decreased as the freezing front moved forward and decreased exponentially with respect to the time of freezing. For the LN_2 bath, as an example, the temperature gradient varied from 65 to 20°C/mm. As a consequence, the freezing rate diminished with the time of freezing. Although the freezing rate changed with time, the direction of freezing or ice growth remained the same. The growth of ice crystals was affected considerably by the magnitude of the freezing temperature. When the freezing bath was changed, the freezing temperature gradient could be changed accordingly and, hence, so could the freezing rate. In our experiment, the order of the freezing rate in the three freezing baths was LN_2 > Freezing EtOH > Freezing EtAc. Because the ice morphology was the template for the SPI molecules, it was important to control the ice morphology as a determining step in the process by controlling the freezing temperature.

The second step was to remove the ice from the system by freeze drying. In this way, the morphology of SPI as a negative copy of the ice template could be easily maintained and successfully made after directional freezing and freeze drying. The freezing rate dependence on the freezing bath was one key factor in determining both the morphology and mechanical properties of the SPI scaffolds.

Morphology

Through the directional freezing process described previously, anisotropic SPI scaffolds with directional morphology could be made. Porosity is an important parameter in foam materials. We measured the apparent volume (the diameter and length) of each scaffold and the solid volume occupied by the soy protein (by dividing the mass by the reference density of the soy protein solid materials, which was about 1.2 g/cm^3). Then, the ratio of the two volumes was calculated, and we found that the porosity was very close to $1 - c$, where c is the initial

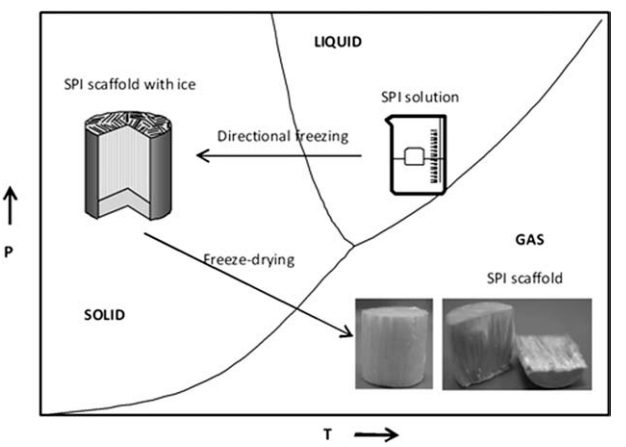

Figure 2 Schematic phase diagram for the preparation of the SPI scaffolds by directional freezing.

concentration of the soy protein solutions. So, we took the initial concentration as the other key factor in addition to the freezing rate when considering the morphological features of the SPI scaffolds. Therefore, in the concentration range 1–10%, the porosity of the scaffold should have been 99–90%. The relationship between the solution concentration and viscosity was discussed in the previous section. We believe that the viscosity of the protein solutions was important in the development of the scaffold morphology as an additional factor in the ice–polymer stability analysis[18] and needs to be examined in a future study.

The morphology of our SPI scaffolds had two distinct zones, a homogeneous zone and a unidirectional zone. The term *homogeneous* refers to three-dimensional isotropic porous structures, and *unidirectional* refers to anisotropic structures, which here refer to aligned structures along the freezing direction. The homogeneous zone nearest the freezing bath had a maximum length of about 2 mm and had a porous microstructure, like scaffolds made with the standard sol–gel process[28] in which the pores are not interconnected. The morphology at this zone was simply an example of isotropic foams, which one can obtain by putting the solutions directly into LN_2. We found that these isotropic pores were smaller with lower freezing bath temperatures, but we did not choose to formulate a general pore size–temperature relation as part of this study. The most interesting section of the morphology was the uniaxial zone. Through control of the concentration of the initial SPI solution and the freezing conditions, a series of different morphologies of SPI scaffolds were obtained.

As shown in Figure 3, when the initial concentration was around 1%, the SPI grew into fibrils. When the concentration was increased to about 4%, those fibrils began to link and formed lamellae; as the concentration increased to 7%, the lamellae became thicker and ridges started to grow normal to the lamellae and with approximately the same spacing as that between the lamellae. Once the concentration reached 10%, the ridges grew to meet the adjacent lamellae to form the new morphology of a cellular structure, which became more complete as the concentration increased. As the concentration increased, the soy protein solutions tended to gel. The scaffolds could also be obtained from the gelling systems of soy proteins with the same technique; however, the morphology was a homogeneous porous structure without any preferred structural alignments. This could be explained at least qualitatively by the linear stability analysis put forward by Zhang et al.,[18] although the secondary ridge morphology is too complex for that model to predict at this stage. These ridges probably contributed significantly to the good performance of the scaffolds in the mechanical tests; this was in agreement with Deville et al.'s[16] suggestion about the beneficial effect of roughness, patterns, and architectures.

Different freezing baths also influenced the morphology of the SPI scaffolds. Here, we use the concentration group of 4% as an example. The freezing bath determined the magnitude of the temperature gradient. With lower bottom temperatures, the temperature gradient was higher, and the forces to push the ice growing in a definite direction were greater. Although the freezing bath was freezing EtOH (−96°C), as shown in Figure 3(e), the resulting scaffold was shown to have a less regular morphology; the lamellae were not so planar as those frozen from the nitrogen freezing bath. When the freezing bath was freezing EtAc (−50°C), as shown in Figure 3(f), the lamellae were smaller, and the ridges seemed to disappear, although the differences between ethyl alcohol and acetate were far smaller than either relative to nitrogen. This observation could be explained by the driving force (which pushed the ice planes or pillars forward and separated SPI from the ice) decreasing as the temperature of the freezing bath was raised.

Because of the size of the samples in the freezing direction, we simply chose a central position from which to observe the morphology. In principle, we should have been able capture the morphological changes as a function of distance along the freezing direction because we were aware of the freezing rate gradient. However, morphology differences along the freezing direction were small compared with the differences between the three freezing baths in the central position. In future studies, investigators should perhaps try to make a more general relation between the freezing rate gradient and morphology, but this was beyond the scope of this study.

Zhang et al.[18] showed that for poly(vinyl alcohol) solutions, the cell diameter normal to the freeze axis decreased at higher freezing rates through an instability wavelength of the periodic ice structure that was governed by the competition between the destabilizing solute interfacial concentration gradient and the surface energy that opposed the cell formation, although the equally important effect of concentration was not demonstrated. Madihally and Matthew[17] showed a more general set of effects for chitosan of the freeze gradient and concentrations of 1 and 2%, in which higher freezing gradients and concentrations both reduced the cell diameter very strongly.

The general evolution of the morphology with both these variables has not been reported so far, and Figure 4 shows a schematic diagram of the evolution of the cellular morphology of SPI with the concentration and freezing conditions in this study

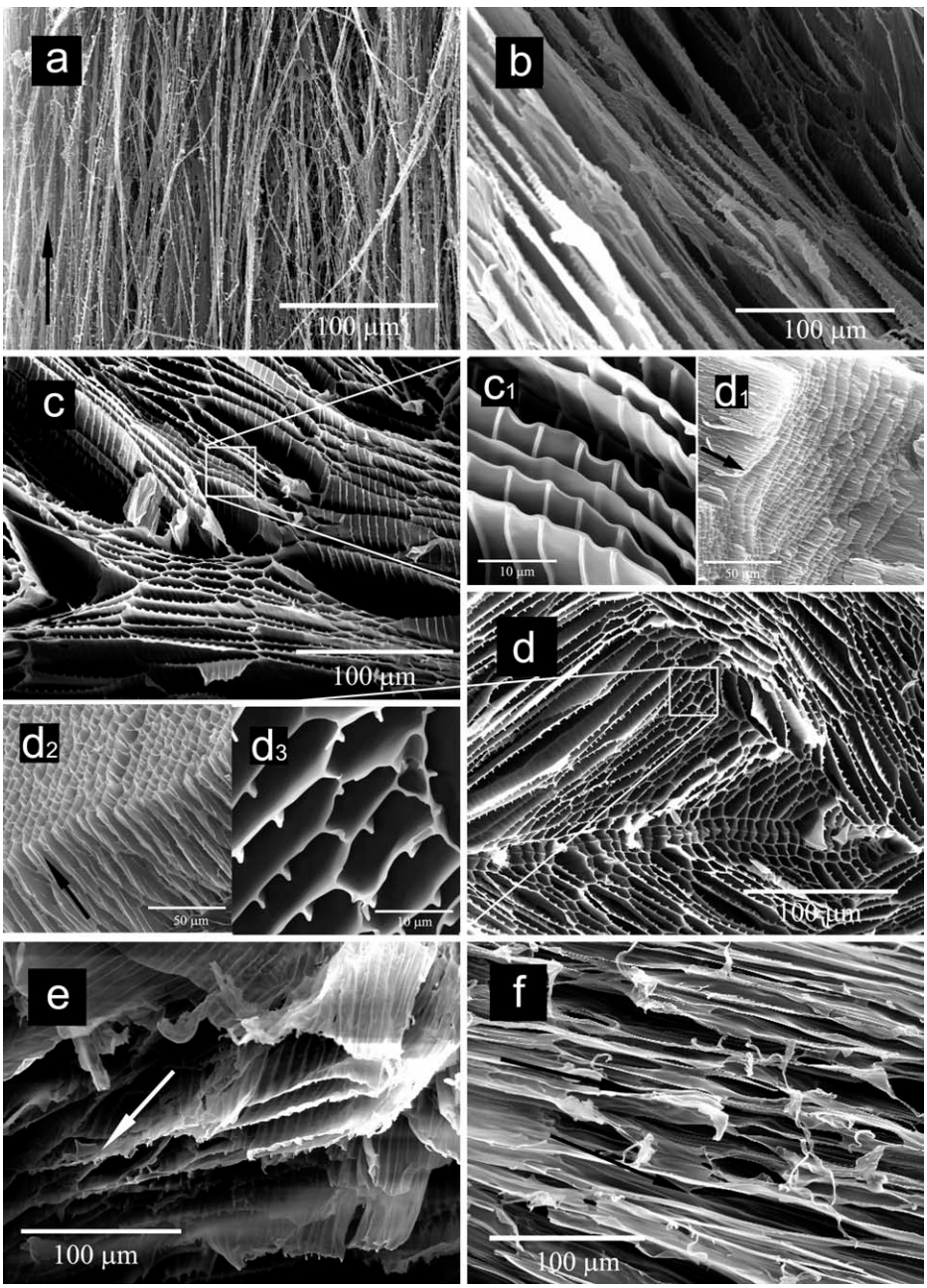

Figure 3 Scanning electron microscopy images with the morphological features of the SPI scaffolds with different initial concentrations and different freezing baths: the initial concentrations were (a) 1,(b,e,f) 4, (c) 7, and (d) 10%. The freezing baths were (a–d) LN_2, (e) freezing EtOH, and (f) freezing EtAc. (c_1) and (d_3) are magnifications of (c) and (d), respectively, and (d_1) and (d_2) are different perspectives of (d). The arrow shows the ice growth direction or the longer axis direction. All of the pictures shown in this figure were taken in the middle of each sample, 5–7 mm from the bottom or the contact side with the freezing baths.

from a large number of observations of morphology at different positions in the samples because the local freezing gradients decreased further from the freezing bath, both along the freezing direction and from the outside to the inside of the samples. As a very rough guide to morphological dimensions with the nitrogen freeze bath, the distance between the lamellae and ridges seemed to have a stable value of about 4 μm, and the density increase at higher concentrations was achieved by a combination of increased lamellar thickness and the growth of the ridges, such that the cell walls had a thickness of about 0.25 μm. The growth of these different morphological features with increasing density determined the relation between the material stiffness and density, which is discussed later. We have also observed, from the X-ray diffraction spectra, that the crystal fraction in the SPI material seemed to

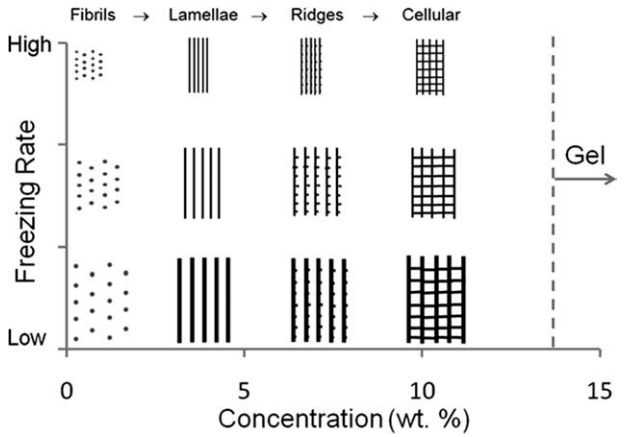

Figure 4 Schematic diagram of the evolution of the morphology normal to the freezing axis with the concentration and freezing rate in this study. A reference scale of dimensions would be about 4 μm for the spacing between the lamellae and ridges at high rates with the nitrogen freezing bath.

increase with increasing concentration but the freezing conditions seemed to have little influence, although we were not able to quantify this effect and interpret its potential effect on the stiffness of the SPI solid material in the cell walls. Additionally, the X-ray diffraction data outside this article show little crystallinity or extreme molecular orientation in the foams, so we, therefore, simply described the polymer as isotropic within the cell walls of the coarser macroscopic oriented pore morphology.

Mechanical properties

Figure 5 shows the typical stress–strain measurements under compression of the SPI scaffolds in the freezing direction and also in the perpendicular one. The cylinder sample was directly used for unidirectional compression, whereas cut scaffolds (obtained under the same conditions as the other direction) with dimensions of $10 \times 6 \times 5$ mm^3 were used for perpendicular compression. All of the samples, despite their initial concentration (except for 1%, which was too weak for compression), had similar stress–strain profile shapes in the freezing and perpendicular directions, but the stress–strain profiles in the two directions appeared to be very different. In the freezing direction, the curves appeared to have a very similar form to those of standard amorphous polymer glasses, albeit with considerably lower magnitude. The perpendicular direction behaved more like a rubberlike elastomer, and the curve shape was similar to that shown by porous natural materials, such as cork;[29,30] it was also remarkably similar to the postyield behavior in the freezing axis.

Figure 6 shows the average value of modulus in the freeze axis as a function of density, and the experimental data split into two separate groupings of the nitrogen and the ethyl alcohol and acetate freezing baths. Here, the apparent density of the scaffolds was determined simply by measurement of the apparent volume (diameter and length) and the mass of each scaffold. The modulus in the freeze axis was proportional to the density (ρ_s) squared in the scaffold over the range of concentrations, freezing temperatures, and different morphologies. This looked remarkably like the standard Gibson–Ashby relation for isotropic open-cell foams with a solid density of $\rho_s = 1300$ kg/m^3 and with a solid modulus value of 2.2 GPa for the nitrogen freeze bath, which was reasonable for a protein with a small crystal fraction and a water content of about 10% determined by thermogravimetric analysis.[31,32]

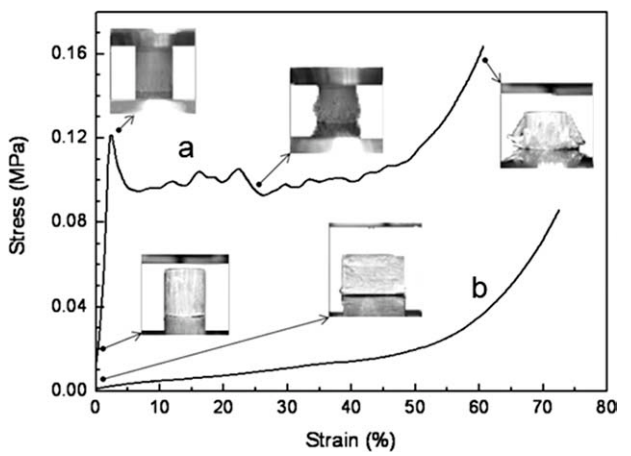

Figure 5 Typical stress–strain curves under compression (a) aligned with the growth direction and (b) perpendicular to the growth direction (initial concentration = 4%, the freezing bath was LN_2). The inserted pictures show the deformation of the scaffolds at different stages.

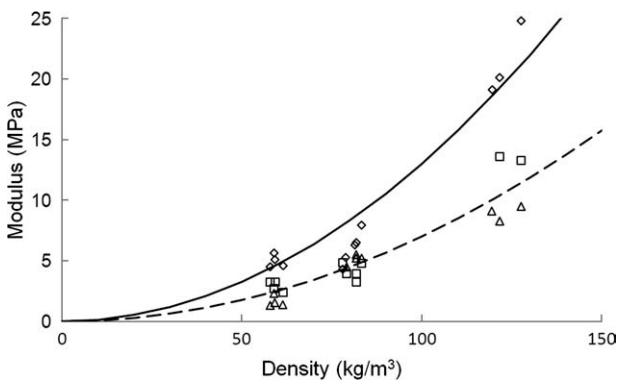

Figure 6 Compression modulus as a function of the density of the SPI scaffolds. The points are the experimental data obtained from different freezing baths: (◇) LN_2, (△) freezing EtOH, and (□) freezing EtAc. The curves are the best fits to the data with a density squared approximation with proportionality constants of 0.0013 and 0.0005 for (—) the LN_2 bath and (- - -) the other two baths, respectively.

Because the morphology of the materials was essentially uniaxial in the freeze direction, we initially expected the modulus in that axis to have a simple linear dependence on density. However, the morphology was not perfectly uniaxial, and the fibrils, lamellae, and tubes were slightly curved and so behaved more like bending beams. The rigidity of such beams depends on the bending moment, which in turn, has a complex dependence on the cross sectional shape of the beam. Models for the axial loading of bent fibers or beads could, in principle, be derived for ideal general morphologies of ribbed lamellae, but the complex distribution of sizes and orientations in the scaffold morphologies put it beyond the scope of this study; for example, the model by González and Llorca[33] for bent fibers illustrates the complexity of such models. However, at a qualitative level, ribbed structures are usually modeled as combinations of rectangular beams, which will have averaged sums of linear and cubic functions of beam thickness and width. As in the Gibson–Ashby standard treatment of open-cell foams, these dimensions can be translated directly into the foam density relative to the solid polymer density, and the squared relation between modulus and density would be a reasonable expectation.

The plateau value of the yield stress in the freeze direction is shown as a function of the modulus in Figure 7. A simple linear relation with a gradient of 0.04 fit the full dataset quite well and, again, was in good agreement with the approximate gradient of 0.05 suggested by Gibson and Ashby for an open-cell foam[34] or, alternatively, the generic gradient of 0.03 for the yield stress of amorphous polymer glasses found empirically by Seitz,[35] which would

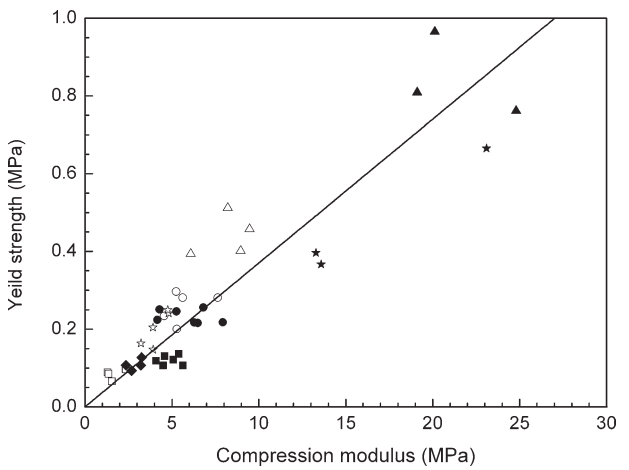

Figure 7 Yield strength against the compression modulus for the full dataset of different SPI scaffolds obtained under different conditions: (■) LN_2 4%, (▲) LN_2 7%, (●) LN_2 10%, (□) freezing EtOH 4%, (△) EtOH 7%, (○) EtOH 10%, (◆) freezing EtAc 4%, (☆) EtAc 7%, and (★) EtAc 10%. The line shows the best fit to the full dataset.

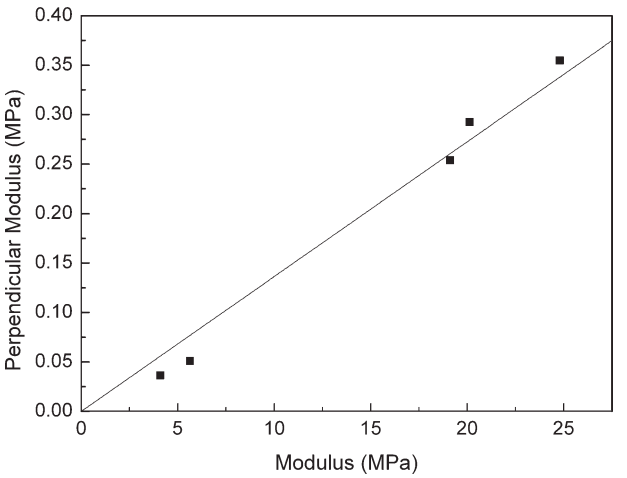

Figure 8 Relation between the values of the modulus in the two test directions. The line shows the best fit to this dataset. All of the data were collected from scaffolds obtained from the LN_2 freezing bath. The initial concentration of the three high modulus points was 10%, whereas the rest was 4%.

be a more materials base for the yield events rather than the more structural suggestion of buckling columns.

Although our dataset was quite limited at this stage, the ratio of modulus in the two measurement directions shown in Figure 8 appeared to be linear and have a constant value of about 0.015 over a wide range of data. New models are required to explain the detailed scaffold properties, with some general hints at possible directions. Given that the shape of the stress–strain profiles was apparently different, this observation was unexpected. If we assume that the scaffolds behaved generically as open-cell foam structures with highly anisotropic cell morphologies, this might be explained with models for anisotropic foams with an aspect ratio of about 6 for the simpler Gibson–Ashby model[29] or 4 for more complex foam geometries.[36,37] We feel that this superficial interpretation is intrinsically flawed, and a more detailed model analysis of the stress–strain relations for the scaffold will be needed to understand the mechanisms; this will be important for future developments in this type of material. Such models will also need to compare axial and transverse loaded bending beams with a general ribbed morphology.

CONCLUSIONS

We showed that robust scaffold materials can be made with soy protein polymer with directional freezing. The morphology of these scaffolds was controlled by a combination of the solution concentration and the rate of directional freezing. Higher concentrations and freezing rates both reduced the

diameter of the cells normal to the freezing axis. In addition, the concentration seemed to have the most control over the development of the scaffold morphology with increasing density. The oriented morphology normal to the freeze axis moved from fibrils at low density (1%) to lamellae (4%) to ribbed lamellae (7%) to cellular (>10%) before an upper limit of concentration of about 12%, where the solution became a gel. We suggest that the evolution of the lamella thickness and rib length with increasing concentration gave a combination of stiffening effects with linear and cubic dependences upon density, such that the resulting density dependence of the axial modulus was (by chance) very similar to that of conventional isotropic open-cell foams. The relations between the axial and perpendicular moduli and the axial yield stress will provide tools for exploring structure–property relations in future studies. A key feature of this study was the use of aqueous soy protein solutions in which the protein chains were well dispersed at neutral pH values to give robust mechanical properties that are usually lacking in soy protein polymers.

The authors thank Xiarong Jiang for sample preparation and Fritz Vollrath, Jinrong Yao, and Lei Huang for their valuable suggestions and discussions.

References

1. Kumar, R.; Choudhary, V.; Mishra, S.; Varma, I. K.; Mattiason, B. Ind Crops Prod 2002, 16, 155.
2. Lu, Y. S.; Weng, L. H.; Zhang, L. N. Biomacromolecules 2004, 5, 1046.
3. Wang, Y. X.; Cao, X. D.; Zhang, L. N. Macromol Biosci 2006, 6, 524.
4. Liu, D.; Tian, H. F.; Zhang, L. N. J Appl Polym Sci 2007, 106, 130.
5. Renkema, J. M. S.; van Vliet, T. J Agric Food Chem 2002, 50, 1569.
6. Renkema, J. M. S.; van Vliet, T. Food Hydrocolloids 2004, 18, 483.
7. Huang, W. N.; Sun, X. Z. J Am Oil Chem Soc 2000, 77, 101.
8. Huang, W. N.; Sun, X. Z. J Am Oil Chem Soc 2000, 77, 705.
9. Zhang, J. W.; Jiang, L.; Zhu, L. Y. Biomacromolecules 2006, 7, 1551.
10. Mungara, P.; Chang, T.; Zhu, J.; Jane, J. J Polym Environ 2002, 10, 31.
11. Vaz, C. M.; Doeveren, P.; Reis, R. L.; Cunha, A. M. Biomacromolecules 2003, 4, 1520.
12. Chen, P.; Zhang, L. Biomacromolecules 2006, 7, 1700.
13. Malafaya, P. B.; Silva, G. A.; Reis, R. L. Adv Drug Delivery Rev 2007, 59, 207.
14. Zhang, H.; Cooper, A. I. Adv Mater 2007, 19, 1529.
15. Deville, S.; Saiz, E.; Nalla, R. K.; Tomsia, A. P. Science 2006, 311, 515.
16. Deville, S.; Saiz, E.; Tomsia, A. P. Biomaterials 2006, 27, 5480.
17. Madihally, S. V.; Matthew, H. W. T. Biomaterials 1999, 20, 1133.
18. Zhang, H. F.; Hussain, I.; Brust, M.; Butler, M. F.; Rannard, S. P.; Cooper, A. I. Nat Mater 2005, 4, 787.
19. Guan, J.; Tian, K.; Yao, J. R.; Shao, Z. Z.; Chen, X. Acta Polym Sinica 2010, 2, 250.
20. Arrese, E. L.; Sorgentini, D. A.; Wagner, J. R.; Anon, M. C. J Agric Food Chem 1991, 39, 1029.
21. Greene, R. F.; Pace, C. N. J Biol Chem 1974, 249, 5388.
22. Loo, J. A.; Edmonds, C. G.; Udseth, H. R.; Smith, R. D. Anal Chem 1990, 62, 693.
23. Adachi, M.; Takenaka, Y.; Gidamis, A. B.; Mikami, B.; Utsumi, S. J Mol Biol 2001, 305, 291.
24. Maruyama, N.; Salleh, M. R. M.; Takahashi, K.; Yagasaki, K.; Goto, H.; Hontani, N.; Nakagawa, S.; Utsumi, S. J Agric Food Chem 2002, 50, 4323.
25. Kinloch, A. J.; Young, R. J. Fracture Behaviour of Polymers; Applied Science: London, 1983.
26. Krevelen, D. W. Properties of Polymers; Elsevier: Amsterdam, 1990.
27. Tanford, C. J Am Chem Soc 1962, 84, 4240.
28. Caillard, R.; Remondetto, G. E.; Mateescu, M. A.; Subirade, M. J Food Sci 2008, 73, C283.
29. Gibson, L. J.; Ashby, M. F. Proc R Soc London Ser A 1982, 382, 25.
30. Huber, A. T.; Gibson, L. J. J Mater Sci 1988, 23, 3031.
31. Porter, D.; Vollrath, F. Soft Matter 2008, 4, 328.
32. Fu, C. J.; Porter, D.; Shao, Z. Z. Macromolecules 2009, 42, 7877.
33. González, C.; Llorca, J. Int J Solids Struct 2005, 42, 1537.
34. Gibson, L. J.; Ashby, M. F. Cellular Solids: Structure and Properties; Cambridge University Press: Cambridge, England, 1999.
35. Seitz, J. T. J Appl Polym Sci 1993, 49, 1331.
36. Sullivan, R. M.; Ghosn, L. J.; Lerch, B. A. Int J Solids Struct 2007
37. Ridha, M.; Shim, V. P. W. Exp Mech 2008, 48, 763.